Clemson University
TigerPrints

All Theses | Theses

5-2011

# Predictive Modeling of Wind Turbine Blades

Kendra Van buren
*Clemson University*, klvan@clemson.edu

Follow this and additional works at: https://tigerprints.clemson.edu/all_theses

 Part of the Civil Engineering Commons

Recommended Citation
Van buren, Kendra, "Predictive Modeling of Wind Turbine Blades" (2011). *All Theses*. 1098.
https://tigerprints.clemson.edu/all_theses/1098

This Thesis is brought to you for free and open access by the Theses at TigerPrints. It has been accepted for inclusion in All Theses by an authorized administrator of TigerPrints. For more information, please contact kokeefe@clemson.edu.

# PREDICTIVE MODELING OF WIND TURBINE BLADES

---

A Thesis
Presented to
the Graduate School of
Clemson University

---

In Partial Fulfillment
of the Requirements for the Degree
Master of Science
Civil Engineering

---

by
Kendra Lu Van Buren
May 2011

---

Accepted by:
Dr. Sez Atamturktur, Committee Chair
Dr. Nadarajah Ravichandran
Dr. John Wagner

# ABSTRACT

Wind turbine blades are being produced at a larger scale in order to meet demands from the burgeoning U.S. wind energy industry, and are forecasted to only grow larger for off-shore applications. Modeling and Simulation (M&S) provides a cost and time efficient alternative when studying the structural behavior of blades such as for loading conditions that are too difficult to replicate in laboratory conditions, and for various severity of damage in wind turbine blades. For this reason, M&S will continue to play an indispensible role in understanding the behavior of wind turbine blades and is gradually replacing the traditional test, build and design procedure.

There are two distinct sources that degrade the predictive capabilities of numerical models: (i) imprecision in parameters and (ii) incompleteness and inaccuracy in the way underlying physics is represented. The first source, also widely known as *known unknowns*, can be remedied by *parameter calibration*. Parameter calibration aims to reduce the uncertainty of the model parameters to the nominal but unknown value that should be used, effectively improving the predictions of the numerical simulation. The second source, also widely known as *unknown unknowns*, can be remedied by *bias correction*. Bias correction accounts for the inherent error that exists in numerical modeling due to the inability of a model to replicate all of the physics of a system.

Herein, the levels of accuracy of the finite element models of two wind turbine blades are rigorously and quantitative assessed. By investigating the sources of uncertainty, this study aims to promote the use of M&S as a reliable tool in future studies of wind turbine blades.

# DEDICATION

I would like to dedicate this study to my grandmother, Hing-Chun Chan.

TABLE OF CONTENTS

Table of Contents (Continued)

LIST OF FIGURES

List of Figures (Continued)

LIST OF TABLES

# CHAPTER ONE

# INTRODUCTION

A better understanding of wind turbine blade vibrations is necessary in the development of wind energy as a viable, unsubsidized source of energy. Modeling and simulation offers a competitive alternative by offering a cheaper alternative to the tradition test, build, and design process. In order, however, to provide dependable results from M&S sources that degrade the predictive capabilities of numerical models need to be identified and rigorously quantified. In an effort to contribute to the future development of wind turbine blades, this study will look into two such sources: (i) incompleteness and inaccuracy of physics and (ii) imprecision in parameters.

The first part of this thesis presents a study on inherent inability of numerical models to completely replicate reality due to unknown or missing physics associated with numerical modeling of wind turbine blades, i.e. *unknown unknowns*. Five alternative finite element (FE) models are developed with varying levels of physics sophistication, and evaluated considering the root stress and tip displacement. The predictive capabilities of the FE models are quantified through the *predictive maturity index*, which requires that the inherent incompleteness and inaccuracy of the model is assessed.

The second part of this thesis presents a study that uses *parameter calibration* applied to a FE model of the CX-100 wind turbine blade. Model calibration involves determining the nominal values that should be used for input parameters to a numerical simulation. The parameters that are changing are known; therefore, uncertainty is due to *known unknowns*. To fully develop the predictive capabilities, sources of uncertainty in the model are understood and quantified through the use of **V**erification and **V**alidation exercises, which aims to

provide credibility for the FE model. The validated FE model is then used to investigate common damage scenarios in wind turbine blades, demonstrating the competitive advantage that numerical modeling offers over costly experimental campaigns.

CHAPTER TWO

# A COMPARATIVE STUDY: PREDICTIVE MODELING OF WIND TURBINE BLADES


## ABSTRACT

For wind turbine blade modeling, vastly different modeling strategies with varying levels of model sophistication are routinely implemented. However, neither the level of sophistication supplied by different modeling strategies nor their predictive capabilities has yet been justified through quantitative and scientifically defendable metrics. This manuscript investigates the necessary level of model sophistication needed for modeling the cross-sections of wind turbine blades by: i) rigorously quantifying the model form error associated with alternative modeling strategies and ii) comparing their predictive maturity index (PMI). The concepts are illustrated on five alternative finite element (FE) models of a prototype blade developed with varying model sophistication. The most sophisticated model, utilizing bi-axial composite layers and orthotropic material properties, is idealized as the *baseline*. Four alternative models are developed by incrementally reducing the model sophistication of the material cross-section, with the least sophisticated model using an isotropic, smeared cross-section. The model form error and PMI associated with the four less-sophisticated models are calculated to establish a comparison with respect to the baseline. While model form error is observed to stay constant for varying levels of sophistication, through PMI it is found that less sophisticated FE models may have predictive capabilities comparable to more sophisticated, computationally expensive models.

*Keywords*: Predictive Capability; Verification and Validation; Bayesian Inference; Uncertainty Quantification; Fidelity to Data; Test-Analysis Correlation

## 1. Introduction

In an effort to address the nation's energy security and carbon footprint concerns, the U.S. Department of Energy intends to produce 20% of energy capacity from wind power by 2030[1]. Consequently, to meet this ambitious goal, the burgeoning wind industry will need to improve the continuous reliability of wind turbines by reducing unavailability due to failures. Wind turbines designed for a life span of 20 years, in the U.S., typically fail on average 2.6 times per year within the first 10 years of their life span[2], with most failures attributed to the gearbox, the generator, and the blades [3]. However, failure of the blade often results in catastrophic damage to the entire wind turbine system [4].

The blades are the critical component in the load transfer within a wind turbine system, generating the entire amount of energy derived from the structure[5, 6, 7, 8]. Thus, wind turbine blades are particularly susceptible to failure because of exposure to turbulence and the wake from other wind turbines[9, 10]. Moreover, due to the increased potential for power output, the current trend is toward manufacturing larger blades with more sophisticated designs[11]. To accommodate the next generation wind turbines, modeling and simulation (M&S) will become increasingly important to validate future blade designs.

M&S offers a more economical and faster alternative to the traditional test, build, and design procedure; however, the predictive capability of models are limited by the uncertainty in calibration parameters, and the *discrepancy bias* due to either incomplete and/or inaccurate

modeling. A review of pertinent literature (see Section 2.1) reveals that there is little uniformity in the development of accurate FE models of wind turbine blades. Thus, in the absence of generally applicable guidelines, vastly different modeling strategies with varying levels of model sophistication are routinely implemented with limited justification.

The purpose of this manuscript is to explore and quantify the effects of simplifications to the modeling of a prototype FE model of a 44-meter Suzlon S88-2.1 MW Type AE-42E wind turbine blade. FE models are developed using NuMAD, preprocessing software developed at Sandia National Laboratories, with a representative geometry of the Suzlon wind turbine blade approximated from in-field measurements. The most sophisticated model (henceforth referred to as the *baseline model*) utilizes orthotropic materials and a composite cross-section, requiring 90 material dependent input parameters. Four alternative models with less sophistication are subsequently developed, in which the model with least sophistication uses an isotropic, smeared cross-section, needing only 20 input parameters. Simplifications to the material cross-sections degrade the models in two fundamental forms: *model form error* increases and the number of input parameters decreases. The model form error represents the fundamental incompleteness and inaccuracy of the model and is overviewed in Section 2.2. A proof of concept example that discusses the effect of model form error on predictiveness of numerical models is provided in Section 2.3.

Section 3.1 overviews the development of five FE models of the prototype blade. Section 3.2 discusses the findings of the solution verification study performed to determine the appropriate mesh size that yields a sufficiently small discretization error. Verification studies are necessary to ensure that estimates of model form error are not contaminated with numerical errors. In Section 4, using the synthetic displacement and root stress data

generated through the baseline model, surrogate models are trained for four less sophisticated models to represent the model form error over the entire domain of applicability. In Section 5, the PMI, a quantitative metric used to establish the predictive capabilities of FE models, is calculated for each model. Section 6 provides a discussion of findings, an overview of the underlying premises, and the limitations of the presented approach.

## 2. Background

Developing simulation models of wind turbine blades offers a faster and more economical alternative to building and testing blades during the design phase. This, however, introduces a new paradigm of how to create accurate predictive models for wind turbine blades. In that regard, a cursory review of efforts in M&S of wind turbine blades is provided in Section 2.1. Model form error, a concept essential to this paper, is introduced in Section 2.2 and demonstrated with a proof of concept example in Section 2.3.

### 2.1 Review of Pertinent Literature

Different modeling strategies have been utilized to study the behavior of wind turbine blades. Such methods include the use of shell and brick elements in a linear analysis[12], or shell and brick elements in a non linear analysis [13]. In addition, to reduce the computational cost of an analysis, beam property extraction methods that can represent three-dimensional elements with one-dimensional line elements were investigated[14]. Diverse modeling strategies are still being proposed, such as when a new element formulation was suggested[15], or when a reduced-order method was proposed to forgo the FE method[16]. This lack of

uniformity in wind turbine blade modeling was highlighted in a previous study [11], when it was emphasized that the choice for the level of detail associated with numerical models is up to the judgment of the analyst.

Recently, there has been an interest to compare the predictive capabilities of common blade modeling strategies with varying model sophistication. These earlier studies, however, were limited to qualitative comparisons. Reference 17 compared the use of shell and 2-dimensional solid models to evaluate the response of a box girder of a wind turbine blade to a compressive line load. While, the main advantages cited for using a simpler model are a reduction in computational time, and the increased ease to perform parametric studies; no set guidelines for how the researcher should determine the appropriate level of complexity needed for the model were discussed. Both shell and solid models used in the study were deemed sufficient, except that geometric non-linearity became a limiting factor when deflections were comparable to the laminate thickness. In 2010, the tradeoffs of using a 2-dimensional beam property extraction technique versus a 3-dimensional modeling for wind turbine blades were investigated[8]. While 2-dimensional section analyses were found to be appropriate for preliminary design, the authors suggest that 3-dimensional models are necessary for more detailed investigations of blades.

Developing a blade model with fewer calibration parameters is of course preferable for reducing complexity and computational cost provided that the model is capable of capturing the behavior of interest. Though the desire to implement simpler models is prevalent for wind turbine blade modeling, limited progress has been made to justify the use of less sophisticated models through quantitative, repeatable and scientifically defendable metrics.

### 2.2 Model Form Error

Reducing the number of input parameters is beneficial as parameter calibration can be kept to a manageable size, lessening the demand for experimental campaigns. However, the reduction in input parameters often comes at the cost of reducing the model sophistication and potentially limiting the predictive capability of the model. The resulting model incompleteness or inaccuracy herein is defined as *model form error*. Model form error in this study, is estimated as proposed in Reference 18 and referred to as *discrepancy bias* (Eq.1). Discrepancy constitutes our best estimate of model form error and is defined as the difference between physical reality and model predictions that cannot be further reduced via parameter calibration. In reality, the 'true' discrepancy between predictions and truth (i.e., model form error) are only known at discrete settings where experiments are available and thus, must be estimated for untested settings. For this study, discrepancy is estimated using a fully Bayesian interpretation in the formulation by Reference 19, to train Gaussian Process Models (GPM). A GPM is a specific type of surrogate model, also known as an emulator or meta-model, which maps inputs to outputs as a purely mathematical function. The algorithm used herein has two goals: i) to train a fast running *simulation GPM* of the relationship developed from the simulation inputs and outputs, and ii) to train a *discrepancy GPM* between the simulation and experimental results. The principles of GPMSA are deeply rooted in the below equation:

$$y_{obs}(x) = y_{sim}(x;\theta) + \delta(x) + \varepsilon^{Test} \quad (1)$$

where $y_{obs}(x)$ are the physical or observed measurements, $y_{sim}(x;\theta)$ are the model predictions, $\delta(x)$ is the discrepancy term, and $\varepsilon^{Test}$ is the measurement error. In Equation 1, x represents

control parameters, which are factors that can be controlled during an experiment. These parameters define the domain within which the FE model is expected to make accurate predictions. The calibration parameters are represented by θ, which are parameters that are input to the FE model but not observed during experimentation. The important difference between control parameters and calibration parameters is that calibration parameters cannot be controlled during experiments.

### 2.3 Model Sophistication: Proof of Concept

This section presents a proof of concept numerical example to demonstrate the reduction in discrepancy from improved model sophistication. Herein, first, an arbitrary mathematical function is generated to define the "truth". Next, from this truth function, two simulation models are derived by reducing the number of terms. *Synthetic experimental observations* are obtained using the "truth" function at five randomly selected points, at x = 50, 150, 200, 250, 300. Here, we discuss the predictive capabilities of two distinct models with different levels of model sophistication: crude model ($y_{sim1}$) and a refined model ($y_{sim2}$).

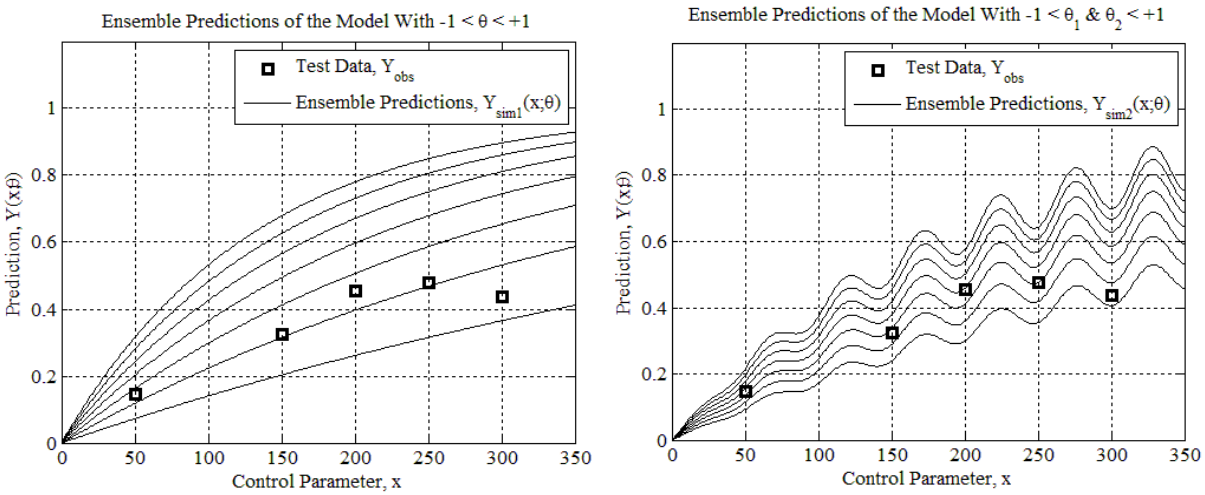


Figure 1: Ensemble Plots of the Model Predictions for ysim1 (left) and ysim2 (right)

The crude model, $y_{sim1}$ has only one calibration parameter, $\theta_1$, which varies between 0 and 1. The left plot of Figure 1 shows an ensemble of crude model predictions obtained by varying $\theta_1$ within its upper and lower limits. The ensemble predictions from $y_{sim1}$ are unable to reproduce the five experimental observations. This inability is because the mathematical function for $y_{sim1}$ is lacking essential terms (and thus essential input parameters) that are present in the truth function. The incompleteness of $y_{sim1}$ results in the discrepancy $\delta_{y1}$ as shown in Figure 2. In an attempt to obtain a refined model with improved model sophistication, a new calibration parameter ($\theta_2$) is added to formulate $y_{sim2}$. By allowing both $\theta_1$ and $\theta_2$ to vary within their predefined ranges, a new ensemble of refined model predictions is obtained as shown in the right plot of Figure 1. Although improved in its model sophistication, the refined model ($y_{sim2}$) is still incomplete and has an associated discrepancy bias ($\delta_{y2}$) as shown in Figure 2. The mean of ensemble predictions for $y_{sim1}$ and $y_{sim2}$ are shown in Figure 2, with the corresponding plots for discrepancy, $\delta_{y1}(x)$ and $\delta_{y2}(x)$. The improvement in predictive abilities of the second model can be visually observed in Figure 2, wherein the function of the refined model, $y_{sim2}$, is able to better capture the behavior of the truth function compared to $y_{sim1}$.

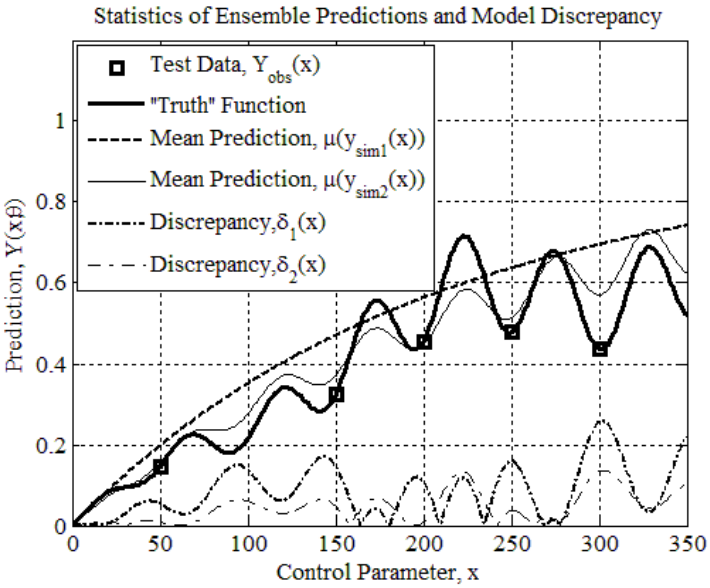


Figure 2: Comparison of "Truth" Function, Mean Predictions, and Discrepancies

In this numerical example, the truth function is known, making it possible to calculate the 'true' discrepancy (i.e., model form error) as the overall distance from the model output and truth function. In Figure 2, the corresponding mean discrepancy, $\delta_{y1}(x)$ is equal to 8.9% of the mean "truth" while the mean discrepancy of the second model prediction, $\delta_{y2}(x)$, is 4.6% of the mean "truth." The increased sophistication of model $y_{sim2}$ allows for a reduction in discrepancy and more adequate predictions of the synthetic data. However, the fact that $y_{sim2}$ has more uncertain input parameters compared to $y_{sim1}$ cannot be overlooked as more uncertain parameters may translate to more uncertainty in the predictions.

## 3. Model Development and Verification

Verification is the process of identifying sources of numerical uncertainty due to programming mistakes, deficient implementations of algorithms and models (code verification) and the spatial and temporal discretization of continuous equations (solution

verification). In this section, the development and solution verification of the FE models are discussed.

### 3.1 Model Development with NuMAD

NuMAD, pre-processing software developed at Sandia National Laboratories, is utilized to create the three-dimensional FE model of a prototype wind turbine blade with Shell281 elements in ANSYS v.12. The Shell281 elements currently utilized in ANSYS v.12 were developed in response to a code verification study that brought into question the ability to properly model torsional bending[20], and recently verified[21] for their performance in bending, torsion, and modal analysis with closed form solutions applied to a hollow cylinder.

Figure 3: Measuring the Wind Turbine Blade

The blade used herein is 44 meters long with a representative geometry of a Suzlon S88-2.1 MW Type AE-42E wind turbine blade. The prototype blade dimensions are approximated from on-site measurements of the Suzlon wind turbine blade located in Texas, as shown in Figure 3. Airfoil profiles available from the National Renewable Energy Laboratory are approximated from the measurements in the absence of design airfoils for the cross-sections. The material composition of the prototype blade is modeled using material lay-ups similar to that of the CX-100 wind turbine blade developed at Sandia National Laboratories[22]. Using these material lay-ups, a baseline FE model is created, in which the cross-section is modeled using orthotropic materials and a composite lay-up with bi-axial layers. Both isotropic and

orthotropic materials can be input into NuMAD, and can in turn be used to create composite layers of specific thickness. The prototype blade herein is modeled by defining different cross-sections at a specific distance from the root, hereby known as a station, as shown in Figure 4. The airfoil, twist of station, chord length, and distance from the root of the blade are specified at each station. The stations are then divided into material sections, to which different composite layers are assigned. The internal structure of the shear web is modeled by connecting delineation points through the airfoil cross-sections of the blade. In order for the prototype blade to be modeled with accurate geometry, nine stations with different material lay-ups are used. The shear web is idealized as having a constant thickness, with the height changing as the blade tapers. Five material sections are defined and represented in Figure 5: the root, the spar of the blade, the trailing edge, the leading edge, and the internal shear web that is not shown.

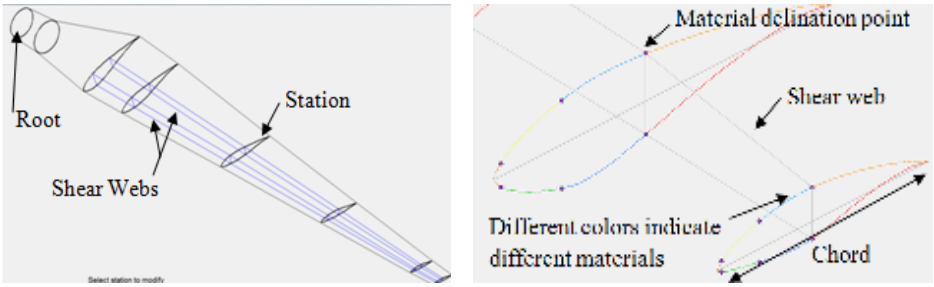


Figure 4: Wind Turbine Blade Development in NuMAD

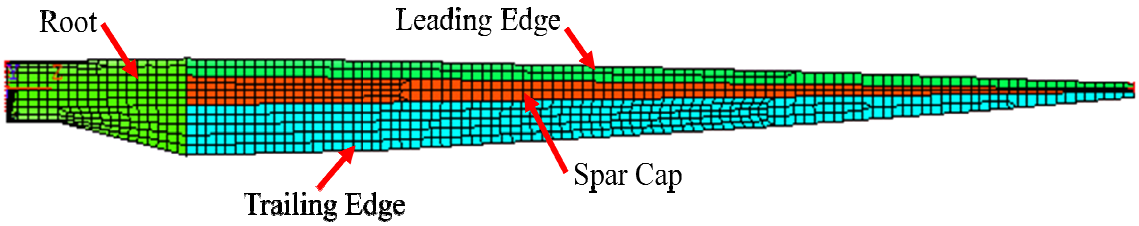


Figure 5: ANSYS Model Showing Different Sections of the Blade

Several assumptions about the material composition of the blade cross-section are needed to simplify the cross-section. To simplify the model from a bi-axial composite cross-section to a uni-axial composite, all of the materials are assumed to have no rotation, effectively creating a cross-section with all of the composite layers oriented in the same direction. To assume an isotropic cross-section, the Young's Modulus used in the x- direction is assumed for the y- and z- directions. To convert the model from a composite to a smeared cross-section, the rule of mixtures for composites is applied, which is a method for computing a characteristic Young's Modulus, Poisson's ratio, density, and thickness for a composite, so that only one layer is needed to model the cross-section[23]. In an effort to limit the changes solely due to model form error, all of the values for material parameters are kept consistent between the five alternative FE models.

Table 1: FE Models Developed in ANSYS

| **FE Model** | **Material Properties** | **Lay-Up** | **Layer Orientations** | **Input Parameters** |
|---|---|---|---|---|
| Baseline | Orthotropic | Composite | Bi-Axial | 90 |
| Blade 1 | Orthotropic | Composite | Uni-Axial | 81 |
| Blade 2 | Isotropic | Smeared | N/A | 45 |
| Blade 3 | Isotropic | Composite | N/A | 36 |
| Blade 4 | Isotropic | Smeared | N/A | 20 |

Based on the above mentioned assumptions, FE models of the Suzlon blade with incrementally simplified cross-sections are obtained in multiple steps. First, the bi-axial layers of the baseline blade are rotated so that all of the layers in the cross-section are oriented in the same direction, creating uni-axial layers for the *Blade 1* model. This reduces the number of FE model input parameters from 90 to 81 since the angle by which layers are rotated is now uniform and no longer needs to be defined. For Blade 2, the rule of mixtures for

composites is applied; this assumption creates a uniform cross-section for each material section. Hence, the number of parameters reduces from 81 to 40. Blade 2 is further simplified by defining the composite layers with isotropic material properties (i.e. eliminating the Young's Modulus in the y- and z- directions). This reduces the number of FE model input parameters to 36 since fewer values are needed to define the material properties. Blade 4 is created by applying the rule of mixtures to the Blade 3 model, resulting in a uniform cross-section defined with isotropic properties, and this model only has 20 model parameters. The resulting FE models and the corresponding number of necessary input parameters are summarized in Table 1.

### 3.2 Solution Verification with ANSYS

For solution verification, a mesh convergence study is performed, by which the mesh of the FE model is successively refined to determine the optimum mesh size. A proper mesh refinement should yield a solution that converges to an asymptote, so that if the FE model is further refined there is minimal gain in solution accuracy. Solution verification is important to ensure that numerical errors have a negligible effect on the estimated model form error.

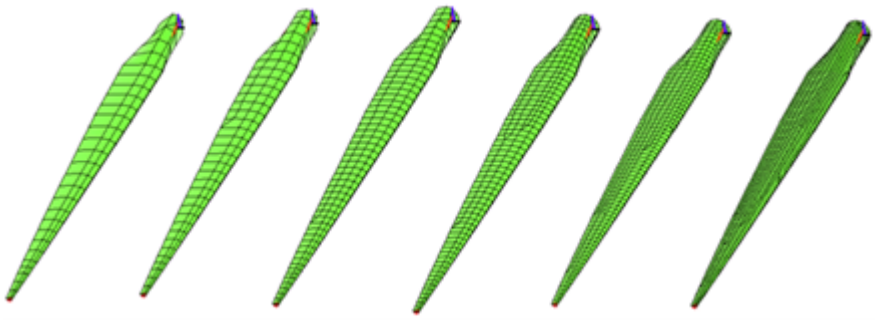

Figure 6: Six Representative Mesh Refinements in ANSYS

The mesh convergence study is performed using static analysis in ANSYS v.12 by observing the stress at the blade root and the displacement of the blade tip due to point loads. The stress and displacements are approximated by averaging over nodes in the region of interest. This is necessary to ensure that the global behavior of the blade is being compared from one FE model to the next. Figure 6 shows six of the forty meshes used to perform the mesh refinement study. The coarsest mesh is shown on the left with 62 elements, and the finest on the right with 10,663 elements, and intermediate levels of mesh discretizations are shown in between. The convergence of the mesh is plotted in Figure 7 for all five blades. A mesh consisting of 2152 elements is chosen for the final FE model, indicated by the vertical black line in Figure 7. The chosen mesh size is within the regime of asymptotic convergence, where only a negligible level of numerical error will be recovered if the mesh is refined.

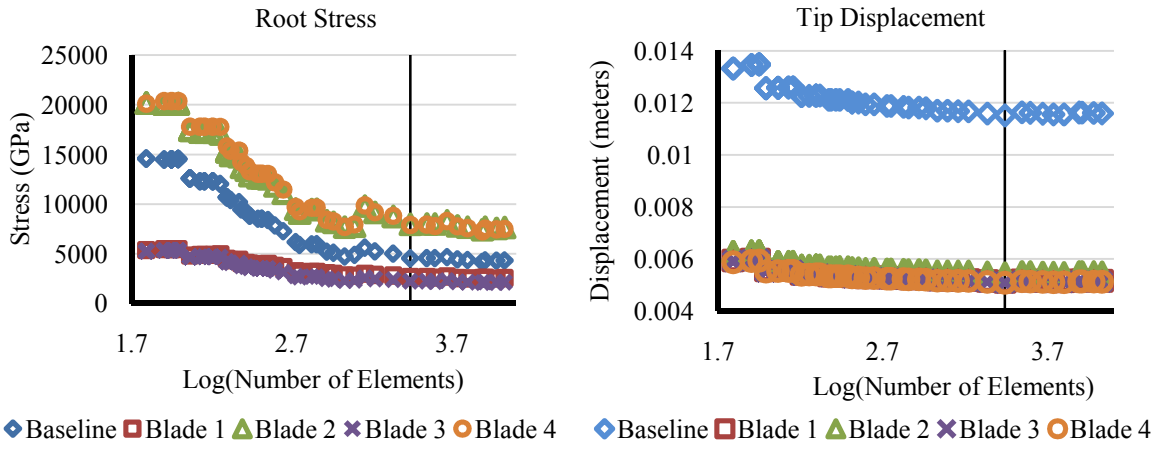


Figure 7: Mesh Convergence of the Root Stress (Left) and Tip Displacement (Right)

## 4. Inferring Model Form Error for the Less Complex Blade Models

The baseline model, being the most sophisticated model, is assumed to represent the 'truth' and used to generate synthetic experimental data. As shown in the top blade of Figure 8, the

synthetic experiments are generated by applying a concentrated point load to ten randomly chosen points on the surface of the blade. The location of each experiment is controlled by the x and z coordinates of the blade. Thus, the x and z coordinates represent the control parameters, while all possible values of x and z represent the entire domain of applicability, which in this study, is the profile of the blade.

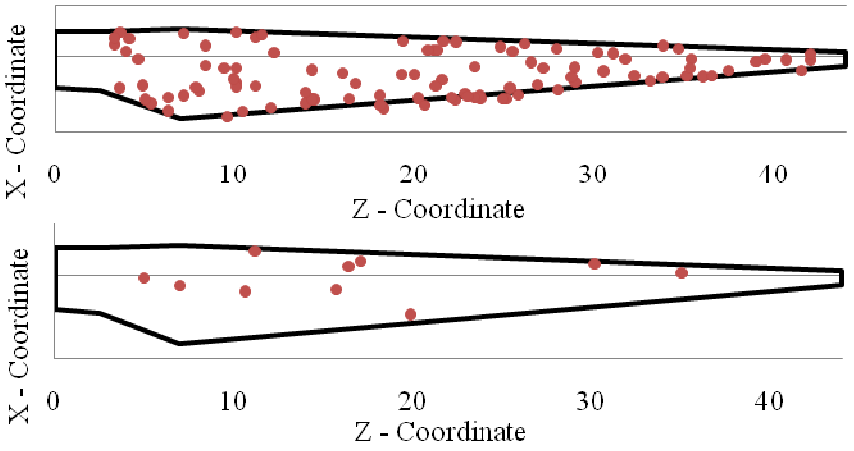


Figure 8: Blade Profile with Observed Data Points (Top) and Simulated Data Points (Bottom)

The synthetic experimental data is used to bias-correct the simulations from the four blade models of lower model sophistication. The bias-correction is straightforward at the ten points where synthetic experiments are available: the bias can easily be calculated as the difference between the synthetic experiments and the less sophisticated model predictions. However, this discrete comparison at ten points only delivers a partial knowledge about the degrading effects of reduced model sophistication on predictiveness of the model. To achieve a complete representation however, one must conduct experiments (in our case, synthetic experiments via baseline model) and obtain model simulations (in our case, by a less sophisticated model) for the entire domain of applicability, i.e. all possible values of x

and z. However, such requirements pose high demands on resources. Especially when the application of interest is not readily amenable to obtain a large number of physical experiments and the simulation model of interest takes a considerable amount of time to complete.

To mitigate these problems, Gaussian Process Models (GPM) are trained using 100 simulations obtained for 100 randomly chosen control parameter pairs, i.e. 100 points on the surface of the blade, as shown in the bottom blade of Figure 8. The *simulation GPM* herein is used as a surrogate to eliminate the need to execute the FE model for the entire domain of applicability. The difference between the FE model and the GPM must be emphasized: while the FE model is developed by the physical relationship of elements and their relationships, a GPM is a surrogate model (also known as meta-model, response surface model) and is a purely mathematical function that defines the relationship between input and output parameters.

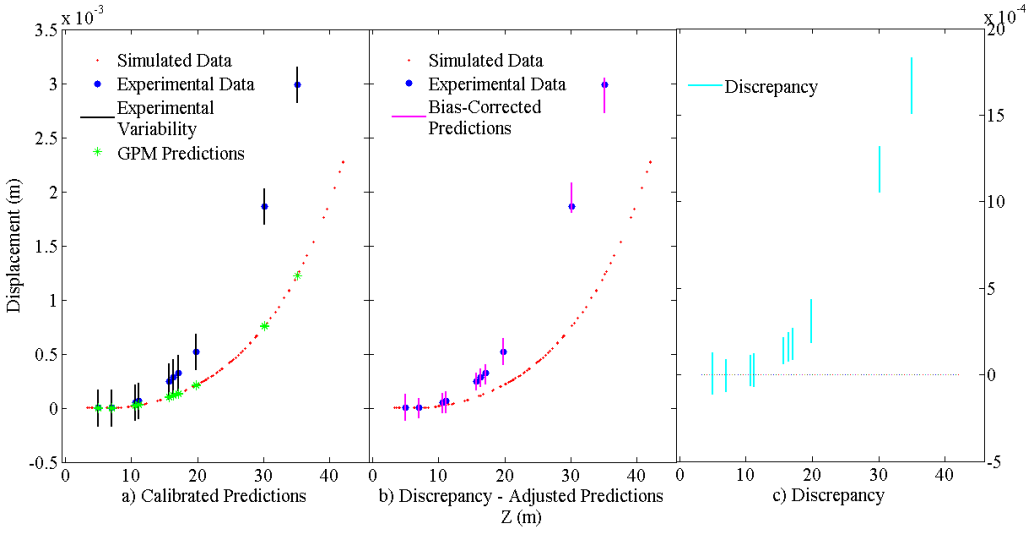


Figure 9: Simulator Outputs

First, a *simulation GPM* is trained for a less sophisticated FE model (recall $y_{sim}(x;\theta)$ in Eq. 1). Next, the synthetic data from the baseline FE model is used to train a *discrepancy GPM* associated with this model (recall $\delta(x)$ in Eq. 1). The procedure is repeated for each of the four alternative modeling strategies. Although several levels of sophistication are removed from the baseline model to develop the four alternative models, the initial step of rotating the bi-axial layers to create a composite blade with layers oriented in the same direction (i.e. from the baseline blade to Blade 1) is observed to have the highest effect on discrepancy. For brevity, the results are presented for Blade 4 only.

In Figure 9-a, the accuracy of the trained *simulation GPM* is confirmed by the agreement shown between the GPM predictions and 100 simulated data. The trained *discrepancy GPM* is non-deterministic in nature, therefore error bars are used to represent the bias-corrected predictions in Figure 9-b. For all ten data points, the experimental data falls within the range of bias-corrected predictions, increasing confidence in the results. The discrepancy at the ten locations of synthetic experimental data are plotted in Figure 9-c.

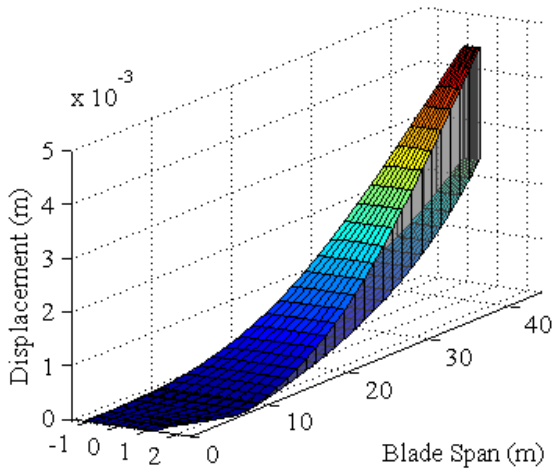


Figure 10: Bias-Corrected Predictions (top) and Calibrated Predictions (bottom)

To obtain a holistic representation of discrepancy, the trained GPMs are used to predict root stress and tip displacement when the concentrated load is applied anywhere on the blade surface, i.e. over the entire domain of applicability. When plotted, these predictions form a surface in a three-dimensional plane, as shown in Figure 10. The volume between the surfaces of *simulation GPM* before and after bias-correction, henceforth referred to as **discrepancy volume**, yields a convenient metric to estimate the level of model form error. The model form error calculated for each blade model are reported in Table 2 for both tip displacement and root stress.

Table 2: Model Form Error of the Blade Models

| **FE Model** | **Volume due to Tip Displacement** | **Volume due to Root Stress** |
|---|---|---|
| Blade 1 | 0.01953 | 11.2E3 |
| Blade 2 | 0.01762 | 25.5E4 |
| Blade 3 | 0.01964 | 13.8E4 |
| Blade 4 | 0.01954 | 20.1E4 |

## 5. Quantifying Predictive Maturity of Alternative Numerical Models

Methods to define the predictive capability of FE models are necessary as modeling and simulation begins to replace the conventional test, build, and design procedure. Recently, a science-based method was proposed[24] to quantify the predictive capability of the model in the predictive maturity index (PMI). The quantitative nature of the PMI is unique in comparison to qualitative methods that have been proposed in the past.[25, 26]

Earlier methods consider the goodness of fit to available experimental data. However, good fidelity to test data of an FE model is only one consideration that needs to be taken into account when defining the predictive capability. This is especially true in cases of over-fitting, in which the FE model has a high fidelity to data, but produces predictions with low

accuracy. Furthermore, it can be shown that the fidelity to available test data and predictive capability of a model have an antagonistic relationship[27]. While model form error, defined in the previous section, is sufficient to quantify the accuracy of the model, the PMI goes a step further in quantifying the predictive capabilities.

Three aspects of the simulation model are considered when defining the PMI: *coverage*, *complexity* of the model, and the *overall level of accuracy*. *Coverage* quantifies how well the available test data covers the domain of applicability. In this study, the coverage is quantified by finding the ratio of the convex hull of the synthetic data to the area of the entire domain of applicability. For the five alternative models investigated herein coverage remains constant because the control parameters of 10 experiments are identical for each blade. *Complexity* is a measure of the level of detail that is used to model the physics. In this study, complexity is quantified by using the number of calibration parameters associated with each model, as reported in Table 1. With everything else equal, if the value used to define complexity increases, the PMI should decrease. This is because a model with an infinite number of parameters is prone to over-fitting, with excellent ability to reproduce experimental data but no predictive capability. The *overall level of accuracy* is quantified using model form error, calculated in the previous section. Not to be confused with goodness of fit, the overall level of accuracy considers the differences between the simulated data and synthetic experimental data that cannot be accounted for by varying the calibration parameters. The final formulation for the PMI metric is given below:

$$\mathrm{PMI} = \eta_c \times \left(\frac{N_R}{N_K}\right)^{\gamma_1} \times (1-\delta_s)^{\gamma_2} \times e^{\left(1-\eta_c^2\right)^{\gamma_3}-\delta_s^2} \qquad \mathrm{PMI} = \eta_c \times \left(\frac{N_R}{N_K}\right)^{\gamma_1} \times (1-\delta_s)^{\gamma_2} \times e^{\left(1-\eta_c^2\right)^{\gamma_3}-\delta_s^2} \quad (2)$$

where $\eta_c$ is the coverage, $N_R$ represents the sophistication of the state of the art, $N_K$ is the sophistication of the model that one is assessing, $\delta_s$ is the measure of goodness of fit[24]. In Equation 2, the $\gamma$ values are user defined coefficients used to weight the effects of various contributions to predictive maturity: $\gamma_1$ weights the effect of the complexity of the model, $\gamma_2$ weights the effect of discrepancy relative to coverage, and $\gamma_3$ weights the interaction between coverage and the overall level of accuracy. The coefficients used to calculate the PMI are $\gamma_1 = 0.5$ and $\gamma_2 = 0.25$, and $\gamma 3 = 10$.

By definition, a PMI of 1 means that the FE model has perfect predictive maturity, and a PMI of 0 means that the FE model has zero predictive maturity. The values of PMI should be used in a relative sense as a comparison between different codes, not as an absolute value. As seen in Table 3, the PMI calculated for each model varies significantly, with the highest assigned to Blade 4 and lowest assigned to Blade 1. The values obtained for the PMI are as expected because, even though Blade 1 has the largest number of calibration parameters, there is no realized gain in predictive capability from the added complexity of the model.

Table 3: PMI Calculated for each Model

| **FE Model** | **Tip Displacement PMI** | **Root Stress PMI** |
|---|---|---|
| Blade 1 | 44.6% | 47.2% |
| Blade 2 | 60.7% | 56.8% |
| Blade 3 | 66.8% | 69.7% |
| Blade 4 | 89.7% | 89.3% |

The PMI metric is able to incorporate the trade-offs between the number of parameters used in each model and the discrepancy bias associated with each model. While a more

sophisticated model generally has the potential to capture the underlying physics principles better, it cannot be assumed that such a model has greater predictive capability. It is also important to note that the two smeared FE models, Blades 2 and 4 required 44% less computation time than the baseline Blade model. The reduction in computational demands combined with the decreased number of calibration parameters and higher predictive maturity make FE models that simplify the modeled cross-sections of wind turbine blades potentially attractive to implement.

## 6. Conclusions

The predictive capabilities associated with alternative modeling strategies are investigated through a prototype FE model of a 44-meter Suzlon S88-2.1 MW Type AE-42E wind turbine blade. Four alternative models of wind turbine blades are developed and their predictiveness is compared. The blade model with highest complexity required 90 calibration parameters, whereas the least complex model required only 20 calibration parameters. A solution verification study is completed to ensure that numerical errors do not lead to faulty estimates of model form error. Next, two types of surrogate models are trained: *simulation GPM* and *discrepancy GPM*. The simulation GPM is effective in reducing the number of necessary computer runs while discrepancy GPM is effective in estimating the model form error over the entire domain of applicability (rather than at just the locations of synthetic experimental data). The initial simplification of rotating composite layers to develop a material cross-section with composite layers oriented in the same direction is observed to have the greatest effect on the discrepancy. Due to the comparable model form error estimated for the four alternative FE models, the blade model with the lowest number of

input parameters has the highest PMI. This finding can be explained by the fact that the blade models with higher levels of sophistication fail to predict more accurately.

The quantitative nature of the PMI captures the trade-off between the number of parameters necessary for each model and the discrepancy bias associated with these models. Therefore, PMI is useful for comparing alternative modeling strategies and defending the level of sophistication used in an FE model. Moreover, the PMI would mitigate issues that may arise from over-fitting because it takes into account the predictive capabilities and not just the fidelity to test data.

Even though the lack of experimental data and assuming the baseline model as the truth is a shortcoming of the present study, the objective, quantitative and repeatable procedures presented herein are generally applicable in cases where experimental data is available. Furthermore, in this study the calibration parameters are kept at their nominal values; however, the proposed approach is amenable to incorporate parameter calibration. Even though not emphasized in this manuscript, it should be noted that a thorough sensitivity analysis of the input parameters should also be carried out prior to parameter calibration or bias-correction activities. To reiterate, only the parameters that have a noticeable influence on the output of interest should be considered during the PMI calculations.

Using model form error and PMI to create quantifiable metrics for the predictive capabilities of FE models has the potential to aid in future attempts to model wind turbine blades by scientifically defending the level of complexity necessary for simulations of wind turbine blades. Such quantitative metrics are important to the future of modeling and simulation of wind turbine blades, because the computational cost can be reduced if a less complex model can be found to adequately model wind turbine blade vibrations.

**Acknowledgements**

The authors wish to express their gratitude to Jean-Paul Cane, of Rope Partner, Inc. for providing the on-site measurements and photos of the Suzlon wind turbine blade. Many thanks to Brian Williams from Los Alamos National Laboratory for providing guidance in surrogate models.

**References**

1. Lindenberg, S., Smith, B., O'Dell, K., DeMeo, E., Ram, B., 20% wind energy by 2030: increasing wind energy's contribution to US electricity supply, US Department of Energy Report, 2008.

2. Echavarria, E., Hahn, B., van Bussel, G.J.W., Tomiyama, T., Reliability of wind turbine technology through time. *Journal of Solar Energy Engineering*, 2008, 130(3), 031005-8.

3. Hill, R., Stinebaugh, J.A., Briand, D., Benjamin, A.S., Lindsay, J., Wind turbine reliability: a database and analysis approach, Sandia National Laboratories, 2008.

4. Ghoshal, A., Sundaresan, M.J., Schulz, M.J., Pai, P.F., Structural health monitoring techniques for wind turbine blades, *Journal of Wind Engineering and Industrial Aerodynamics*, 2000, 85(3), 309-324.

5. Ashwill, T., Blade Technology Innovations for Utility-Scale Turbines, Sandia National Laboratories, 2006.

6. Ashwill, T., Laird, D., Concepts to facilitate very large blades, in: *Proceedings, ASME/AIAA Wind Energy Symposium*, 2007.

7. Paquette, J.A., Veers, P.S., Increased strength in wind turbine blades through innovative structural design, in: *Proceedings, European Wind Energy Conference*, 2007.

8. Resor, B., Paquette, J., Laird, D., Griffith, D.T., An evaluation of wind turbine blade cross section analysis techniques, in: *AIAA/ASME/ASCE/AHS/ASC Structures, Structural Dynamics, and Materials Conference*, 2010.

9. Devinant, P., Laverne, T., Hureau, J., Experimental study of wind-turbine airfoil aerodynamics in high turbulence, *Journal of Wind Engineering and Industrial Aerodynamics*, 2002, 90(6), 689-707.

10. Thomsen, K., Sorensen, P., Fatigue loads for wind turbine operating in wakes, *Journal of Wind Engineering and Industrial Aerodynamics*, 1999, 80(1-2), 121-136.

11. Griffith, D.T., Paquette, J.A., Carne, T.G., Development of validated blade structural models, in: *46th AIAA Aerospace Sciences Meeting and Exhibit*, 2008.

12. Bechly, M.E., Clausen, P.D., Structural design of a composite wind turbine blade using finite element analysis, *Computers & Structures*, 1997, 63(3), 639-646.

13. Jensen, F., Falzon, B.G., Ankersen, J., Stang, H., Structural testing and numerical simulation of a 34 m composite wind turbine blade, *Composite Structures*, 2006, 76(1-2), 52-61.

14. Malcolm, D.J., Laird, D.L., Modeling of blades as equivalent beams for aeroelastic analysis, in: *Proceedings of the AIAA/ASME Wind Energy Symposium*, 2003.

15. Alpay, S., Barut, A., Madenci, E., An efficient modeling approach for dynamic simulation of wind turbine blades, in: *AIAA/ASME/ASCE/AHS/ASC Structures, Structural Dynamics, and Materials Conference*, 2010.

16. Murtagh, P., Basu, B., Broderick, B., Mode acceleration approach for rotating wind turbine blades, *Proceedings of the Institution of Mechanical Engineers, Part K: Journal of Multi-body Dynamics*, 2004, 218(3), 159-167.

17. Pardo, D., Branner, K., Finite element analysis of the cross-section of wind turbine blades; a comparison between shell and 2D-solid models, *Wind Engineering*, 2005, 29(1), 25-32.

18. Kennedy, M., O'Hagan, A., Predicting the output from a complex computer code when fast approximations are available, *Biometrika*, 2000, 87(1), 1-13.

19. Higdon, D., Gattiker, J., Williams, B., Rightley, M., Computer model calibration using high-dimensional output, *Journal of the American Statistical Association*, 2008, 103(482), 570-583.

20. Laird, D.L., Montoya, F.C., Malcolm, D.J., Finite element modeling of wind turbine blades, in: *43rd AIAA Aerospace Science Meeting and Exhibit*, 2005.

21. Mollineaux, M., Van Buren, K., Hemez, F., Simulating the dynamics of wind turbine blades: part I, model development and verification, in: *13th AIAA Non-deterministic Approaches Conference*, 2011.

22. Berry, D., Ashwill, T., Design of 9-meter carbon-fiberglass prototype blades: CX-100 and TX-100, Sandia National Laboratories, 2007.

23. Tsai, S., Hahn, H.T., *Introduction to Composite Materials*, Westport, Conn., 1980.

24. Hemez., F.M., Atamturktur, H.S., Unal, C., Defining predictive maturity for validated numerical simulations, *Computers & Structures*, 2010, 88(7-8), 497-505.

25. Balci, O., Adams, R.J., Myers, D.S., Nance, R.E., Credibility assessment: a collaborative evaluation environment for credibility assessment of modeling and simulation applications, in: *Proceedgins of the 34th Conference on Winter Simulation: Exploring New Frontiers*, 2002.

26. Harmon, S.Y., Youngblood, S.M., A proposed model for simulation validation process maturity, *The Journal of Defense Modeling and Simulation: Applications, Methodology, Technology*, 2005, 2(4), 179-190.

27. Hemez, F.M., Ben-Haim, Y., The good, the bad, and the ugly of predictive science, in: *4th International Conference on Sensitivity Analysis of Model Output*, 2004.

# CHAPTER THREE

# PARAMETRIC MODELLING OF DAMAGE IN WIND TURBINE BLADES THROUGH VALIDATED FINITE ELEMENT MODELS

**ABSTRACT**

A parametric study of common damage types of wind turbine blades is detailed through a combined analytical and numerical study. Finite element (FE) model of the CX-100 wind turbine blade is calibrated against experimental measured natural frequencies in a two-staged process focused on the free-free blade and subsequently on the fixed-free blade model. The calibrated FE model is then validated using the mode shape vectors. The validated FE model is used to simulate three common types of damage: leading edge erosion, skin delamination of the trailing edge and adhesive debonding between the shear web and the skin. The location of the onset of damage, varied across the length of the blade and the severity of the damage, is gradually increased from 20 cm to 200 cm. Finally, to quantify the effects of damage, the changes in the natural frequencies were monitored. This work demonstrates the implementation of both verified and validated numerical models for an improved understanding of the structural behavior of wind turbine blades.

**Keywords:** Test-Analysis Correlation, Uncertainty Quantification, Model Calibration, Verification and Validation, Statistical Inference

## 1. INTRODUCTION

Wind energy research is being pursued in the United States as a viable alternative to provide a major amount of installed electrical power, as part of the *"20% by 2030"* initiative by the U.S. Department of Energy. However, if wind energy is indeed to become a mainstay of US energy needs, its cost must be first reduced drastically. According to a report from Sandia National Laboratories (SNL), during the first year of operation the expense of operating and maintaining a wind farm is as low as $5/MWh, whereas over a 20 year evolution of service will climb as high as $20/MWh (Walford 2006). Furthermore, because blade damage to turbines are perhaps the most prohibitive cost of such wind energy (Larsen & Sorensen 2003), condition-based blade maintenance schemes are critical to lowering operational and maintenance. Such schemes are only possible through a better understanding of wind turbine blade vibrations.

Modeling and simulation (M&S) techniques for studying the vibrations of wind turbine blades are absolutely crucial for constructing a new generation of blades and for maintaining current blades in optimal condition because they offer a cheaper alternative to traditional testing, construction and design procedures (Resor et al. 2010). The overarching goal of this study, therefore, is to demonstrate the use of a validated FE model in simulating wind turbine blade damage. A competitive advantage offered by the FE model used in this study is the rigorous **V**erification and **V**alidation (V&V) exercises

undertaken to ensure the predictive capability of the model output. With this validated FE model, common damage scenarios (e.g. leading edge erosion, skin delamination on the trailing edge and adhesive debonding between the shear web and the skin) are simulated. The severity and location of damage are varied and the effects of damage on the natural frequencies are quantified. This study demonstrates the potential of FE models as a tool to predict the behavior of wind turbine blades exposed to damage.

## 2. BACKGROUND

FE models calibrated against experimental data have been developed for routine use in studying wind turbine blade damage, owing to their versatility in predicting many complex load cases (Jensen et al. 2006), whereas only idealized loads can be implemented in full scale experiments (Freebury & Musial 2000). Although the use of FE models has been actively pursued, sources of uncertainty remain, such as an inexact match of geometry to design, a deviation of material properties from coupon properties, and when critical sections exhibit unique stress loading behaviors (Freebury & Musial 2000). Therefore, the benefits of incorporating uncertainty in the model parameters and treating the model predictions in a probabilistic manner are both significant and necessary.

One such example of combined experimental and analytical studies is provided by Sørensen et al.(2004) who performed a full static test to failure of a wind turbine blade to confirm the FE predictions of the buckling behavior of the blade. Similarly, Jensen et al. (2006) successfully developed a finite element model to study the buckling collapse

observed during experimental flap-wise loading of the blade. In subsequent experimentation, Marín et al. (2009) investigated fatigue damage to study why 300 kW wind turbine blades were failing prior to the design life of 20 years. A complete visual inspection of blade samples determined that cracks formed at three main places: when there is an abrupt change of thickness, in the transition area of the blade, and at the site of manufacturing defects. Common manufacturing processes involve fabricating the two skins and shear web separately followed by adhesive bonding of the blades themselves (Cairns et al. 1998). This adhering process relies on a bonded sample that is capable of holding the wind turbine blade together.

Common damage scenarios for wind turbine blades, illustrated in Figure 1 were summarized by Sørensen et al. in 2004. Here, Type 1 damage corresponds to shear web debonding due to the formation of damage in the adhesive layer joining the spar cap and shear web, and Type 2 damage corresponds to the formation of damage in the adhesive layer joining the lower pressure and higher pressure sides of the blade. A more detailed explanation of these two adhesive debonding and erosion damage scenarios with the FE model in detailed in Section 8.

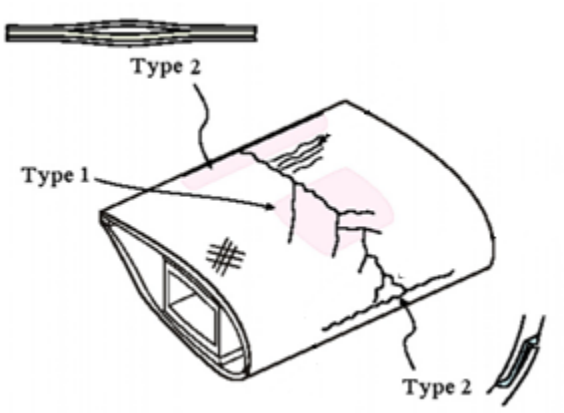


**Figure 1: Sketch of common wind turbine blade damage. (from Sørensen et al. 2004, with permission)**

The various types and severity of damage to wind turbines is often predicated upon the speed and turbulence of the wind, and the topography, and turbulence intensity (Noda & Flay 1999, Sutherland & Kelley 2003, H. J Sutherland et al. 2001). Furthering the difficulty of determining the exact failure mode is that the actual failure locations are unknown and difficult to identify. Failure modes can include skin laminate failure in tension or local buckling, adhesive failure in shear or peel, bolted joint failure (Freebury & Musial 2000), or delaminations with associated cracks and debonding (Mandell et al. 2003). Therefore, to be meaningful any study using simulation to investigate damage must be parametric in nature and consider the inherent variability in damage type, location and severity.

## 3. THE CX-100 WIND TURBINE BLADE

The wind turbine blade used in this study is the CX-100, which is a 9-meter research blade developed at SNL from the Blade System Design Study (BSDS). The purpose of the BSDS is to incorporate high-risk design innovations that may not be economical for industry to carry out in the development and testing of wind turbine blades (Paquette et al. 2006). Achieving these innovations, however, requires reliable M&S techniques so that new design concepts can be evaluated prior to implementation into the wind turbine blades. The design proposed for the CX-100 blade revolves around a full-length spar cap manufactured with a unidirectional carbon-fiber laminate (see Figure 2). The added strength and stiffness from the carbon spar cap is designed to effectively reduce the cost

of operation by increasing the amount of energy produced while reducing the loads applied to the wind turbine system (Berry & Ashwill 2007).

**Figure 2. Carbon spar cap of the CX-100 wind turbine blade (from Paquette & Veers 2007, with permission).**

The CX-100 blade has been heavily studied by testing undertaken at SNL. In 2007, structural testing was performed on the CX-100 wind turbine blade (Paquette et al. 2007). In addition, an experimental modal analysis of a stalled wind turbine system, outfitted with CX-100 wind turbine blades, was performed (White et al. 2010). The analysis confirmed that the boundary conditions of the wind turbine blade affect the obtained mode shapes. There is an evident need to further understand the behavior of CX-100 blades, which is achieved in this study using FE analysis.

## 4. EXPERIMENTAL CAMPAIGN

Modal testing of the CX-100 wind turbine blade is performed under both free-free and fixed-free boundary conditions at the Los Alamos National Laboratory, the details of which are described in (Deines et al. 2011). This work includes a summary of experimental variability due to excitation locations, support conditions, and orientation of

the wind turbine blade. Figure 3 shows the setup of the free-free experimental testing condition (left) and a close-up of the excitation grid used in the modal analysis (right).

**Figure 3. Free-Free modal testing configuration (left) and measurement grid (right).**

Roving impact hammer tests were performed to amass modal data at three locations with uni-axial accelerometers. A linear average was used for five repeats over a 150 Hz sampling frequency. The acceleration response was measured for 11 seconds, during which the response of the blade is attenuated, negating the use of window function. The overall levels of experimental variability observed for the experiments are quantified and listed in Table 1. This variability is attributed to the ability to repeat experiments on one test specimen of the CX-100 wind turbine blade, resulting in very low levels of uncertainty.

**Table 1. Statistics of system identification obtained for the CX-100 blade (from Van Buren et al. 2011, with permission).**

| Statistics of Identified Frequency for Free-free Modal Testing | | | |
|---|---|---|---|
| **Type of Mode** | **Mean Value** | **Std. Dev. Value** | **Variability[(1)]** |
| First flap-wise bending | 7.617 Hertz | 0.004 Hertz | 0.06% |
| Second flap-wise bending | 20.167 Hertz | 0.055 Hertz | 0.27% |
| Third flap-wise bending | 32.256 Hertz | 0.051 Hertz | 0.16% |
| **Statistics of Identified Frequency for Fixed-free Modal Testing** | | | |
| **Type of Mode** | **Mean Value** | **Std. Dev. Value** | **Variability[(2)]** |
| First flap-wise bending | 3.221 Hertz | 0.008 Hertz | 0.24% |
| Second flap-wise bending | 8.824 Hertz | 0.011 Hertz | 0.12% |
| Third flap-wise bending | 19.204 Hertz | 0.020 Hertz | 0.11% |

Legend: Variability is the standard deviation (column-3) divided by the mean (column-2). [(1)]Based on 27 replicates for the free-free tests. [(2)]Based on 47 replicates for the fixed-free tests.

## 5. FINITE ELEMENT MODEL DEVELOPMENT

The FE model of the CX-100 wind turbine blade was developed with the NuMAD preprocessor created at SNL and imported into the ANSYS software. Notably, the material sections were modeled using smeared, isotropic cross-sections, approximated by applying the rule of mixtures for composites to the available manufacturing design specifications of the blade. Previously, the use of these assumptions was justified by Van Buren et al. (2011). A total of six sections were used for the FE model, shown in Figure 4: the shear web, root, spar cap, trailing edge, leading edge, and leading edge with balsa.

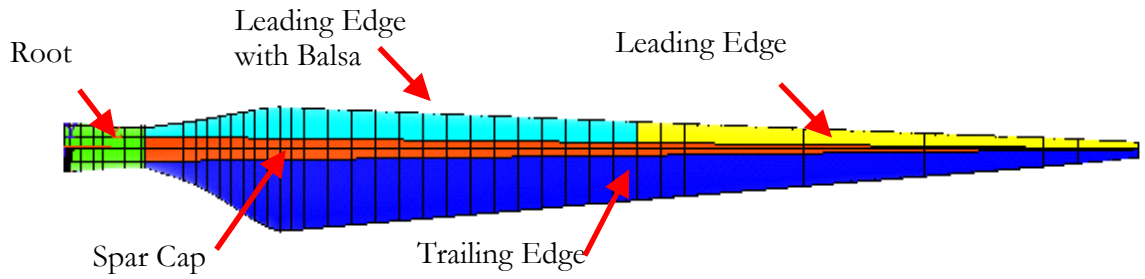


**Figure 4. Different sections of the ANSYS model.**

Code and solution verification activities were performed to ensure that the ANSYS shell-281 elements were properly implemented and provided accurate solutions (Mollineaux et al. 2011). A solution verification was undertaken to choose a mesh size that produces numerical error comparable with experimental variability. A discretization based on an element size of $\Delta x = 8$ cm was found to provide numerical uncertainty of 1.78%, which is comparable to the maximum level of experimental variability obtained by replicating the modal tests ($\pm 3\sigma = 1.62\%$, see Section 4). This mesh counts 3,070 elements and computes the modal solution in less than 30 seconds, which is a constraint that must be met so as to enhance the feasibility of parametric studies.

## 6. SENSITIVITY ANALYSIS, UNCERTAINTY PROPAGATION, AND MODEL CALIBRATION

It is important to understand the influence that both individual, or groups of model parameters exercise on the variability of FE predictions. Understanding which parameters exercise the most influence on model predictions allows for a reduction in parameters used for model calibration exercises. Calibration of the FE model involves a two-step

procedure: i) on the free-free model and ii) the fixed-free model. In this two-step process, the coupling of material properties and boundary conditions are de-coupled. In the first step, the material properties of the blade are calibrated using the natural frequencies of the free-free blade. In the second step, the spring constants mimicking the blade connection to the nacelle are calibrated using the natural frequencies of the fixed-free blade.

### 6.1 Free-Free Simulation

The model is parameterized by twelve inputs, consisting of the Young's Modulus (E) and density ($\rho$) used for the six sections of the blade. A Phenomena Identification and Ranking Table (PIRT), which originated from high-consequence studies on nuclear reactor safety, is developed (Wilson & Boyack 1998). The PIRT provided in Table 2, is used to organize the results of a two-level full factorial analysis, using the upper and lower bounds approximated for the material properties. The $R^2$ values obtained from an Analysis-of-Variance (ANOVA) of the first free bending mode frequencies are used to screen the parameters to the five that account for 95% effect on the variability of the FE model.

**Table 2. PIRT for the free-free analysis (from Van Buren et al. 2011, with permission).**

| Factor | Description | Lower Bound | Upper Bound | $R^2$ Values | Keep? |
|---|---|---|---|---|---|
| A | Shear web, ρ | 650.46 $kg.m^{-3}$ | 1,084.10 $kg.m^{-3}$ | 0.29% | **No** |
| B | Root, ρ | 2,071.56 $kg.m^{-3}$ | 3,452.60 $kg.m^{-3}$ | 0.37% | **No** |
| C | Lower-edge balsa, ρ | 1,025.05 $kg.m^{-3}$ | 1,708.42 $kg.m^{-3}$ | 0.32% | **No** |
| D | Spar cap, ρ | 1,900.44 $kg.m^{-3}$ | 3,167.40 $kg.m^{-3}$ | 1.11% | **No** |
| E | Trailing edge, ρ | 659.04 $kg.m^{-3}$ | 1,098.40 $kg.m^{-3}$ | 9.35% | **Yes** |
| F | Leading edge, ρ | 2,059.68 $kg.m^{-3}$ | 3,432.80 $kg.m^{-3}$ | 3.03% | **Yes** |
| G | Shear web, E | 0.992 MPa | 2.975 MPa | 1.74% | **No** |
| H | Root, E | 18.006 MPa | 54.019 MPa | 0.00% | **No** |
| I | Lower-edge balsa, E | 4.362 MPa | 13.085 MPa | 1.74% | **No** |
| J | Spar cap, E | 31.041 MPa | 93.122 MPa | 65.95% | **Yes** |
| K | Trailing edge, E | 0.917 MPa | 2.752 MPa | 9.85% | **Yes** |
| L | Leading edge, E | 10.304 MPa | 30.911 MPa | 6.25% | **Yes** |
| Total main-effect contribution | | | | 100.0% | |

Legend: The composite $R^2$ statistics shown in column-5 are computed for main-effect screening by averaging individual $R^2$ for mode 1 (1st flap-wise bending), mode-3 (2nd flap-wise bending) and mode-4 (3rd flap-wise bending). Since all parameters exhibit high uncertainty, the uncertainty column in omitted from the PIRT.

After screening the initial 12 parameters down to a subset of the five most significant, an initial test analysis correlation (TAC) of the mode shapes is performed to ensure that (i) the experimental and numerical mode shape are paired and (ii) mode swapping does not occur as the material properties are perturbed. A two-level, full factorial design of experiments is implemented to obtain all combinations of mode shapes from the lower and upper bounds when varying the five sensitive parameters identified in Table 2. The

variation in the mode shapes are plotted in Figure 5. While there is significant variability in the mode shapes, the general behavior remains constant as the parameters are varied.

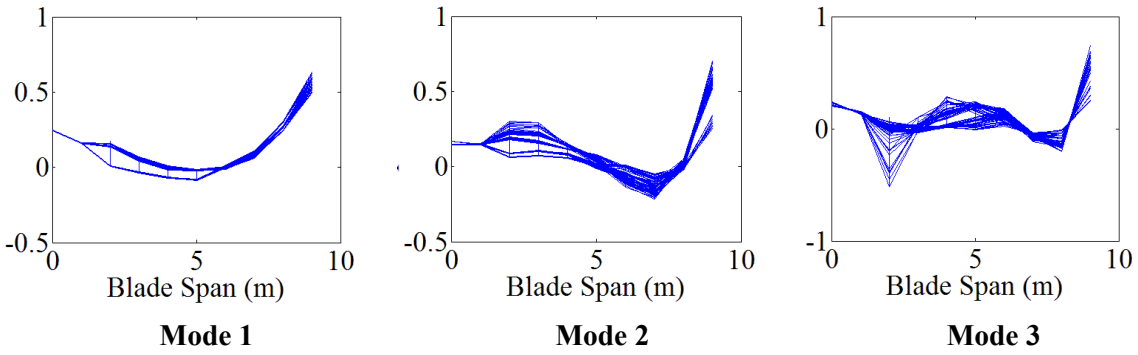


**Figure 5. TAC of mode shapes used for the parametric study**

A three-level, full factorial design-of-computer-experiments ($3^5$ = 243 runs) is analyzed to generate the training data needed to develop statistical emulators and to bias correct the parameter values. In this design, each one of the five parameters is set to a lower bound, nominal value (mid-range) and upper bound. Three levels are defined such that quadratic effects and higher-order interactions can be captured. A Markov Chain Monte Carlo (MCMC) exploration of the unknown posterior distribution of FE model parameters is performed to reduce the range of uncertainty of the parameter values (Higdon et al. 2008). The posterior is, by definition, the probability distribution of the five FE parameters that produces an overall prediction uncertainty that is as similar as possible to the experimental variability. The computational procedure relies on the principles originally proposed by (Kennedy & O'Hagan 2000).

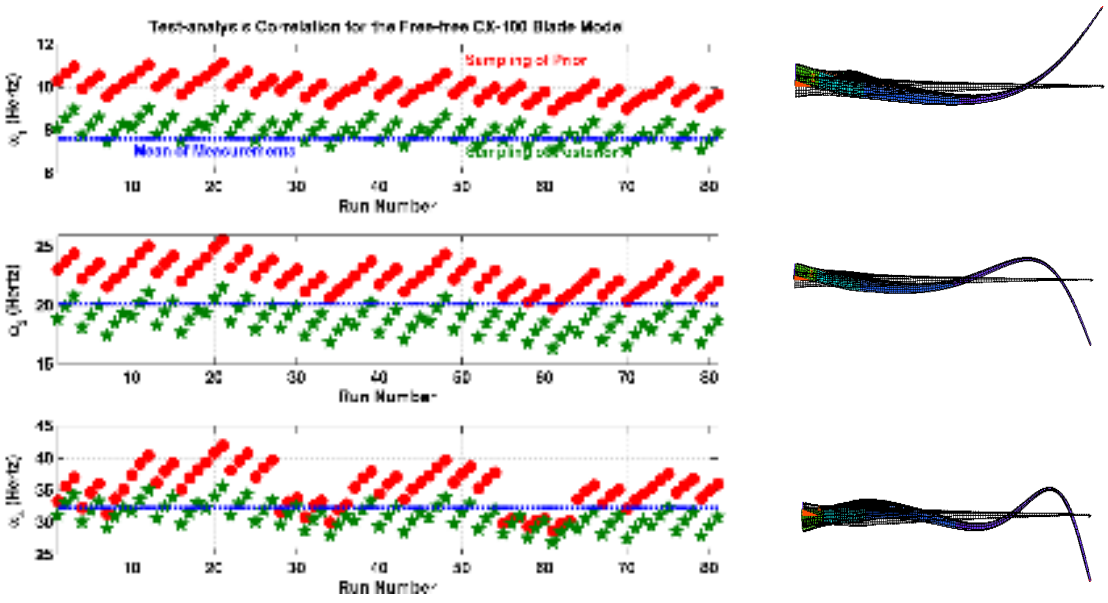


**Figure 6. Comparison between measurements, prior and posterior predictions for the free-free condition of the first three flapwise modes (from Van Buren et al. 2011, with permission).**

Figure 6 compares the mean measurements (dashed lines) to predictions obtained before and after calibration, where the prior ranges (dot symbols) and posterior ±2σ bounds (star symbols) are sampled in ANSYS. Each subplot corresponds to one of the modes of interest for validation. As evidenced by Figure 6, predictions sampled from the posterior distributions more closely agree with the measurements.

### 6.2 Fixed-Free Simulation

The analysis proceeds with the model development and parameter calibration of the fixed-free configuration of the CX-100 blade in which additional springs are added to

represent the boundary condition compliance. The fixed-free condition is implemented experimentally by attaching the CX-100 blade to a steel "bookend" fixture, weighing approximately 500 lbf, shown in Figure 7. Although this fixture is used to create the experimental fixed-end condition, there is an inherent uncertainty introduced due to the unavoidable difficulty in replicating fixed end conditions. Springs were utilized in order to mitigate this uncertainty, and to create a simulation that more closely represents actual operational conditions, i.e. the blade is neither "free" nor "fixed."

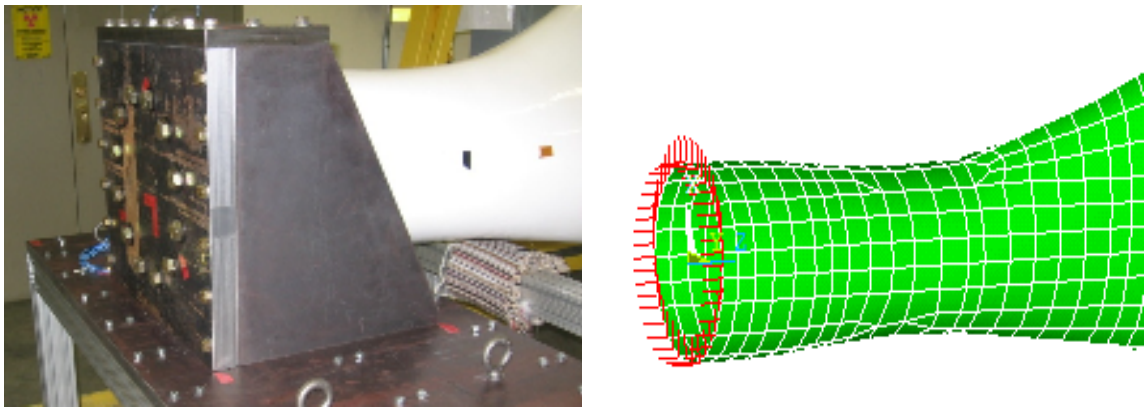

**Figure 7. Close-up of the steel bookend fixture (left) and fixed-free simulation using springs (right).**

Through an effect screening study, the rotational springs at the base of the blade were found to have insignificant effect on the vibration characteristics. Therefore, translational springs are added to the base of the CX-100 blade in the x, y, and z directions at 40 locations around the diameter of the base. The blade behavior asymptotically converges to the fixed-free blade when the spring stiffness constants are sufficiently large and to the free-free blade when the coefficients are sufficiently small.

To reduce the uncertainty associated with the spring stiffness constants a parametric, another parametric study is performed. However, parametric studies on support conditions are prone to mode swapping as the stiffness constants are increased. As shown in Figure 8, a mismatch between the first mode of the simulated free-free blade and fixed-free blade is observed. It can be deduced that the first flap-wise mode of the fixed-free condition is not introduced to the simulation until the springs are sufficiently stiff. Figure 9 shows that as the spring constants were are varied, the first flap-wise mode corresponding to the fixed-free condition occurs once the spring stiffness coefficients achieve a value of approximately $10^6$ N/m. This value constitutes our lower bound for the parametric study.

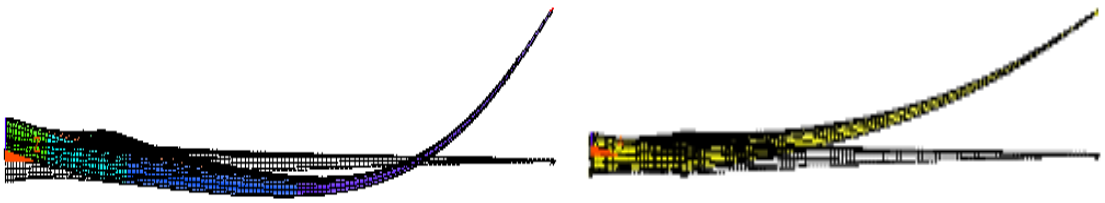

**8-a) First flap-wise mode under free-free (left) and fixed-free (right) conditions.**

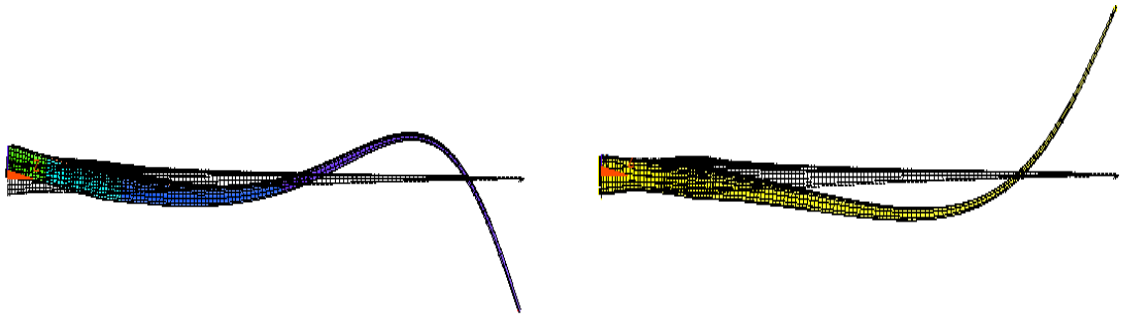

**8-b) Second flap-wise mode under free-free (left) and fixed-free (right) conditions.**

**Figure 8. Comparison of the simulated free-free and fixed-free mode shape deflections (from Van Buren et al. 2011, with permission).**

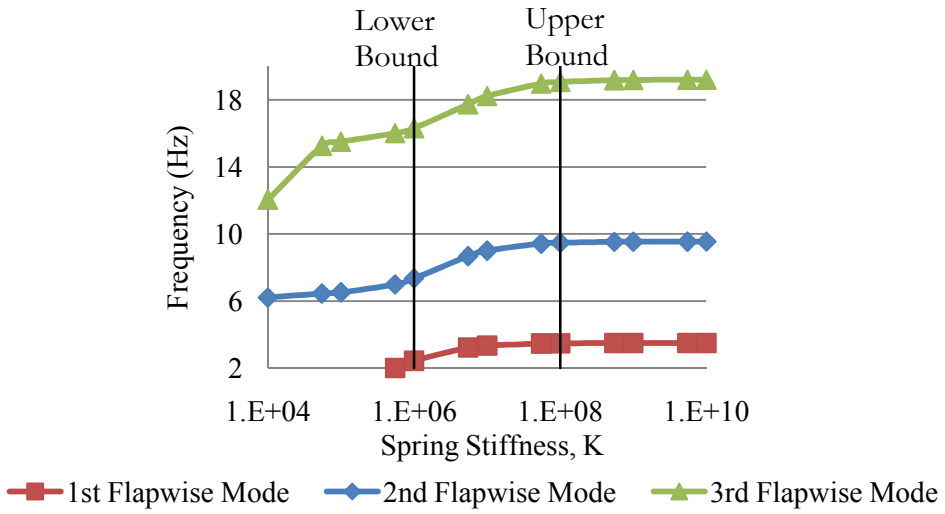


**Figure 9. Variation of the Spring Constants (from Van Buren et al. 2011, with permission).**

Furthermore, the simulations approach a fixed condition at a value of 108 N/m, which is a good upper bound candidate for the parametric study. Table 3 shows that the bending modes predicted from both models have a difference of 0.02 Hz, or approximately 0.1% error for the third flap-wise bending mode. Also note the shape vectors obtained with a$10^8$ N/m stiffness constant that match those obtained with boundary conditions fixed in translation in all directions.

**Table 3: Comparison of frequencies for fixed boundary condition simulations (from Van Buren et al. 2011, with permission).**

| Mode | Fixed-Free Frequency | Rigid Springs Frequency | Description |
|---|---|---|---|
| 1 | 3.49 Hertz | 3.49 Hertz | 1st flap-wise bending |
| 3 | 9.55 Hertz | 9.54 Hertz | 2nd flap-wise bending |
| 5 | 19.23 Hertz | 19.21 Hertz | 3rd flap-wise bending |

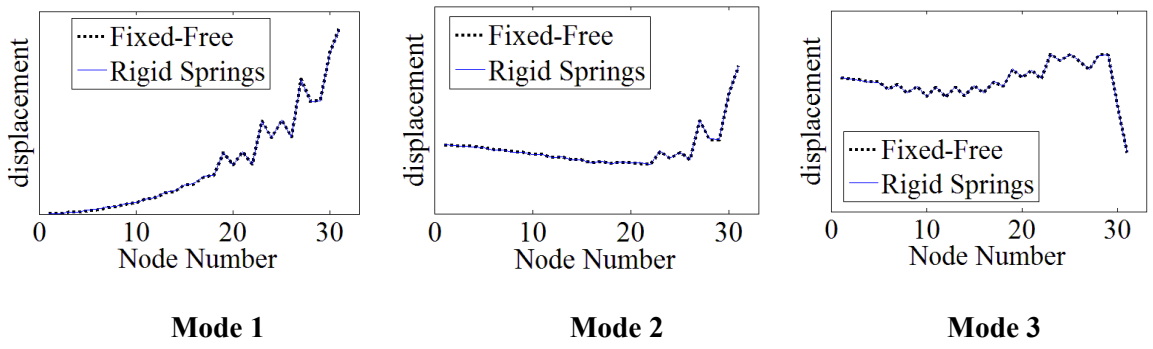


**Figure 10. Comparison of mode shapes for fixed boundary condition simulations**

The final step to developing the FE model of the CX-100 blade for the fixed-free condition involves calibrating the imprecise stiffness constants of the FE model. In this case, a full sensitivity analysis of all blade material properties is unnecessary. Only the parameters that are anticipated to have an effect are evaluated. Note that in the free-free study, the material properties of the root are found to be insignificant contributors to the output variability, whereas in the fixed-free model, the strain energy of the blade is shifted towards the base of the blade. Therefore, a closer investigation of the material parameters of the root is warranted.

The parameters that were found to have a considerable effect on the variability of the free-free model (Trailing Edge Density, Spar Cap Modulus, and Trailing Edge Modulus) are retained for a parametric study for the fixed-free model, along with the spring stiffness constants and the Young's Modulus and density for the root section. The subsequent seven parameters are then used to investigate the variability of the model response.

**Table 4. PIRT for the fixed-free analysis (from Van Buren et al. 2011, with permission).**

| FE Model Parameter | Parameter Lower Bound | Parameter Upper Bound | $R^2$ Statistics of Total Effect | | | Keep? |
|---|---|---|---|---|---|---|
| | | | Mode-1 | Mode-3 | Mode-5 | |
| Root, ρ | 2,072 $kg.m^{-3}$ | 3,453$kg.m^{-3}$ | 0.00% | 0.00% | 0.00% | **No** |
| Trailing edge, ρ | 484.4 $kg.m^{-3}$ | 729.8 $kg.m^{-3}$ | 1.59% | 5.14% | 12.47% | **Yes** |
| Root, E | 18.006 MPa | 54.019 MPa | 0.18% | 0.58% | 0.72% | **No** |
| Spar cap, E | 29.918 MPa | 53.562 MPa | 6.90% | 27.30% | 29.17% | **Yes** |
| Trailing edge, E | 1.484 MPa | 2.348 MPa | 0.07% | 0.15% | 5.17% | **No** |
| XY Springs, K | $10^6$ $N.m^{-1}$ | $10^8$ $N.m^{-1}$ | 0.00% | 0.00% | 0.03% | **No** |
| Z Springs, K | $10^6$ $N.m^{-1}$ | $10^8$ $N.m^{-1}$ | 39.44% | 66.26% | 50.14% | **Yes** |

The results of the sensitivity analysis are shown in Table 4, with three parameters retained for calibration. The material properties of the root are observed to have an insignificant effect on the response of the wind turbine blade when modeled under fixed-free conditions. It is possible that the more dominant parameters simply outweigh the contribution of the material properties of the blade root on the model response. In addition, only the translational springs in the z-direction have a significant effect on the response of the wind turbine blade. This is likely due to the fact that, as can be seen in Figure 9, the range of values used for the spring coefficients constrains the variation in natural frequency. A sensitivity analysis was used to reduce the number of parameters from seven to three. A level four, full factorial parametric study with the same parameter bounds of Table 4 was performed to capture the quadratic effects and obtain training data.

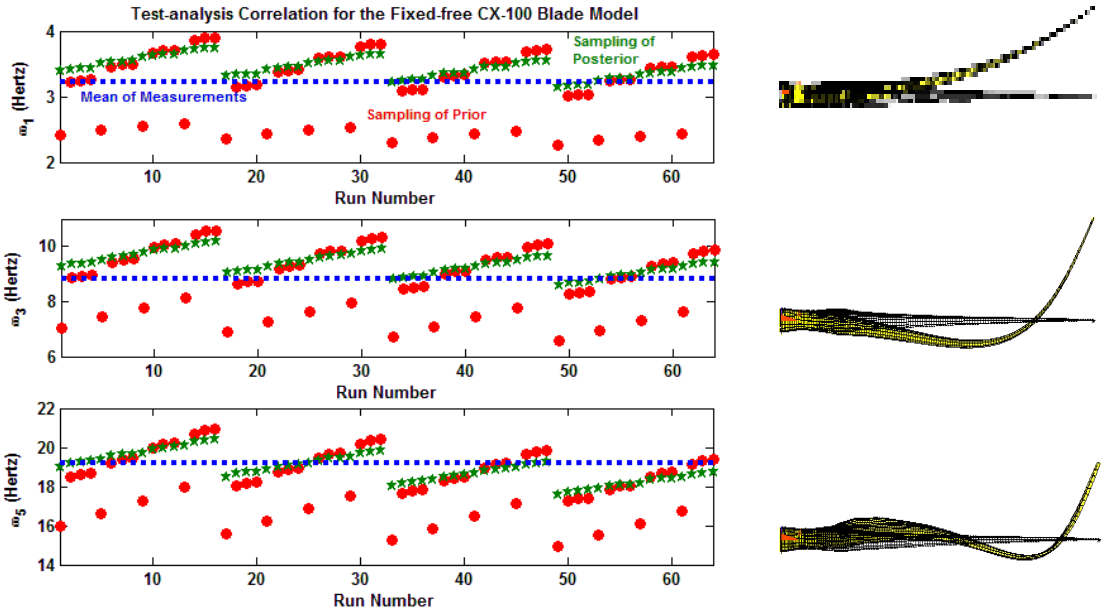


**Figure 11. Comparison between measurements, prior and posterior predictions for the fixed-free condition (from Van Buren et al. 2011, with permission).**

Figure 11 compares the mean measurements to predictions obtained before and after calibrating the material parameters with each subplot corresponding to one of the modes of interest. It can be observed that even though the effect screening was limited to a reduced number of parameters, the resulting sample from the posterior distributions tend to agree better with the measurements.

## 7. MODEL VALIDATION

Recall the FE model is calibrated using solely natural frequencies. In this section, model validation is performed by comparing the mode shape vector that is a separate data set. This is necessary to **validate** the predictive capability of the FE model. The mode shapes are generated

by multiple simulation runs obtained with parameter values sampled from the posterior distributions. Such runs are an important component in the development of an FE model to illustrate that the model can match several aspects of data obtained experimentally. In Figure 12, the experimental mode shape is plotted using a solid line, and the simulation variability is reported with box plots.

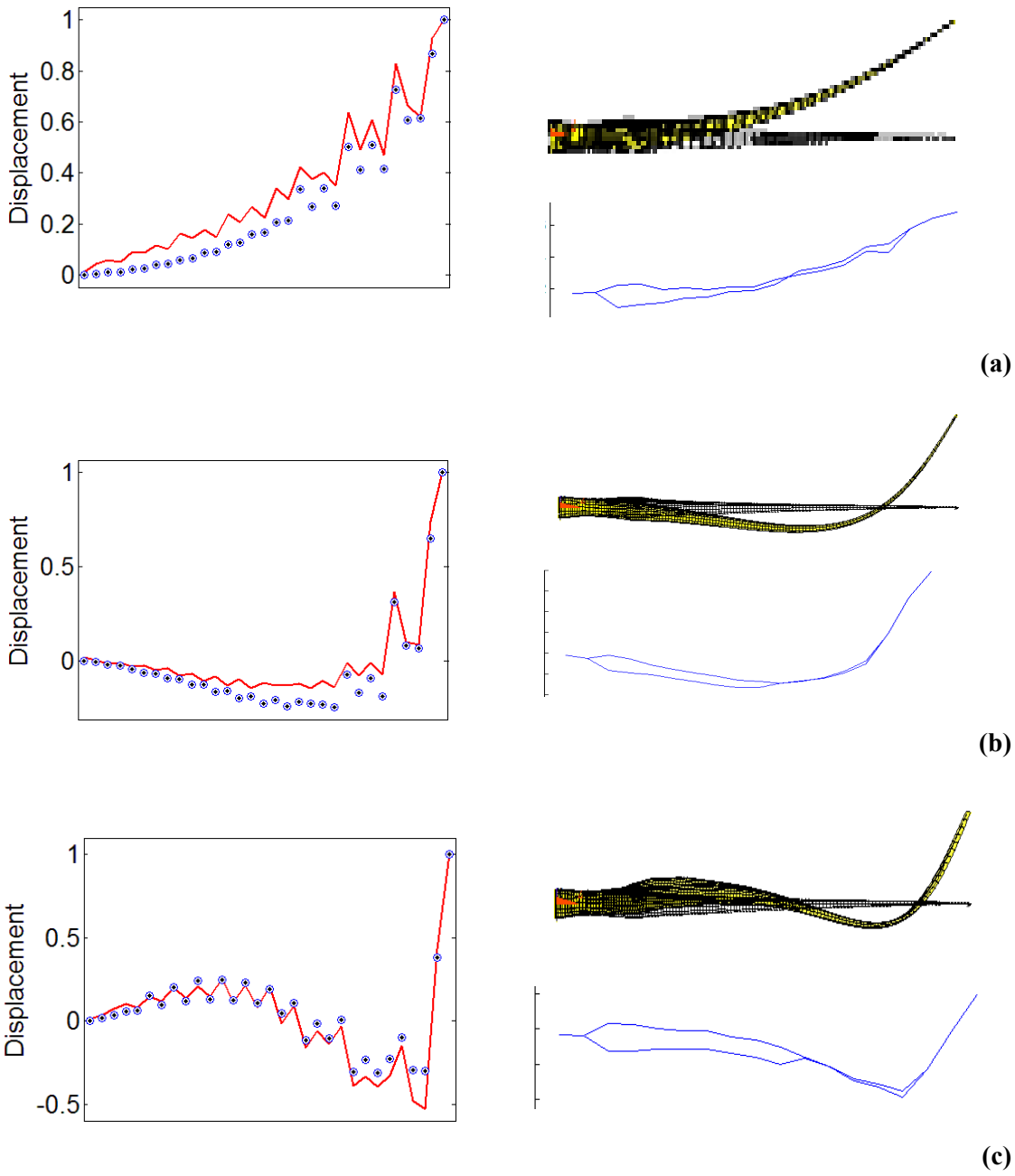


**Figure 12. Comparison of mode shapes (left) compared to the simulated mode shape (upper right) and experimental mode shape (lower right) for (a) Mode Shape 1, (b) Mode Shape 2, and (c) Mode Shape 3 for the Fixed-Free Modes (from Van Buren et al. 2011, with permission).**

## 8. SIMULATING DAMAGE

Damage is introduced to the simulation of the FE model in the form of adhesive debonding of the shear web (Type 1 damage, see Section 2), in which a crack forms where the shear web connects into the spar cap of the wind turbine blade, along either the top or bottom of the shear web. This damage type is of particular importance for the load carrying capacity and structural performance of the wind turbine blade because the spar cap is designed to provide the main structural reinforcement (Cairns et al. 1998). Trailing edge delamination and leading edge erosion (Type 2 damage, see Section 2) is also considered. This results in crack propagation along four areas of the blade: the top and bottom of the shear web, the trailing edge, and the leading edge. To simulate damage, overlapping keypoints are produced at the same location to provide a discontinuity when the model is meshed, effectively creating a crack in the model. Figure 13 shows a comparison of the resulting fifth mode shape from the damaged wind turbine, produced by introducing a 2-m crack along the trailing edge, to the undamaged FE model.

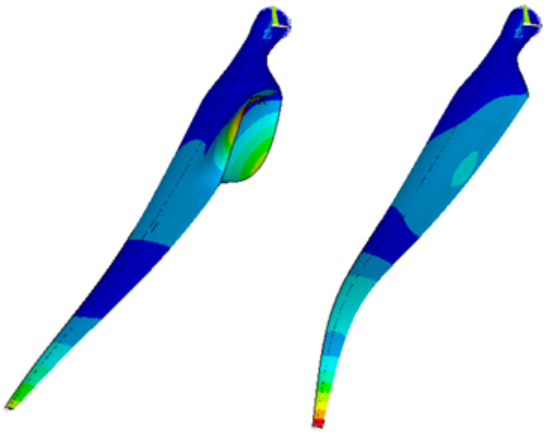

**Figure 13: Mode shape 5 for the damaged (left) and undamaged (right) blade**

Cracks are propagated using varying lengths, from 0.2m to 2.0m, the progressive effects of which are shown in Figure 14, using the natural frequencies of the first five modes.

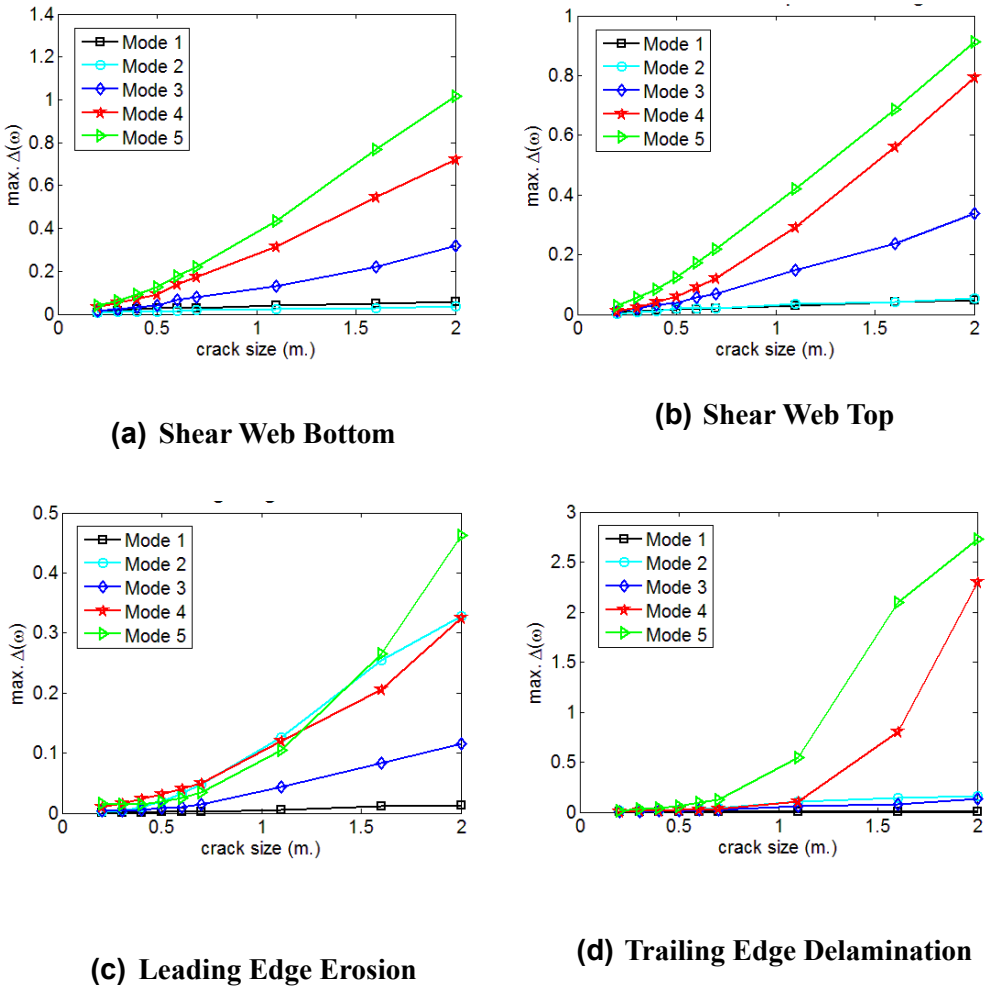


**(a) Shear Web Bottom**

**(b) Shear Web Top**

**(c) Leading Edge Erosion**

**(d) Trailing Edge Delamination**

**Figure 14: Effect of Crack Propagation on Natural Frequencies**

The first three modes of the FE model are robust to the introduction of damage in the FE model. Such robustness is perhaps due to the fact that lower order modes typically represent global behavior of the structure, whereas higher order modes are more sensitive

to localized effects. Cracks simulated in the trailing edge of the wind turbine blade experience a bigger change in natural frequency than cracks simulated in the shear web. Though the effect of damage on the mode shape is obvious from a visual inspection of the mode shapes produced in Figure 13, the change in natural frequencies yield no similar conclusions. This demonstrates the high level of robustness that natural frequencies of wind turbine blades exhibit. In addition, the change in natural frequency depends on the location of cracks. Although 2m-meter cracks were introduced to the 9-meter blade, the change in natural frequency observed for the leading edge erosion and shear web debonding fails to exceed 1Hz, as shown in the plots of Figure 14. It is important to consider that in-field conditions typically introduce noise to the measurements, and that a metric that is more sensitive to damage should be used to detect the onset of damage.

## 9. CONCLUSION

Wind turbine blade damage was investigated through the use of a validated wind turbine blade model in this study. The FE model was developed using design specifications for the CX-100 wind turbine blade. Natural frequencies, obtained through experimental modal analysis, were used in a two-step calibration procedure for the free-free and fixed-free simulations. Model validation was then performed using the mode shapes of the wind turbine blade. The excellent agreement observed in the model validation is attributed to the predictive capability of the FE model. Two damage types, obtained through a literature review, were investigated to observe the potential to investigate damage scenarios in the wind turbine blade. It is emphasized that the

credibility of model predictions due to implementation of damage applied to the wind turbine blade is attributed to the use of a validated FE model. The change in the first five modes is compared, and of the damage scenarios investigated, trailing edge delamination was observed to produce the highest change in natural frequency.

While it is emphasized that M&S provides a cheaper alternative to experimentation, the use of validation data sets are still useful to ensure prediction accuracy of the FE model. Small scale experiments should be performed to better elucidate the components of the wind turbine system, as opposed to large scale experimentation. Future research should entail investigating further damage scenarios in both numerical simulations and experimentally. The work performed in this study relies on the modal behavior of the blade due to the fact that the dynamics of interest in the validation of the numerical model were the bending modes of the wind turbine blade. However, other metrics should be explored to determine better methods to determine both the existence and amount of damage introduced to the wind turbine blade.

## ACKNOWLEDGEMENTS

The authors also wish to express their gratitude to Krystal Deines, Timothy Marinone, and Ryan Schultz, students of the 2010 Los Alamos Dynamics Summer School, for supplying data and photos from the experimental modal analysis of the CX-100 wind turbine blade.

## REFERENCES

Berry, D. and Ashwill, T., 2007. Design of 9-Meter Carbon-Fiberglass Prototype Blades: CX-100 and TX-100, Sandia National Laboratories.

Cairns, D.S, Haugen, D.J., Mandell, J.F., and Samborsky, D.D., 1998. Fracture of skin/stiffener intersections in composite wind turbine structures. In 36th AIAA Aerospace Sciences Meeting and Exhibit. Reno, NV.

Deines, K., Marinone, T., Schultz, R., Farinholt, K., Park, G., 2011. Modal Analysis and SHM Investigation of CX-100 Wind Turbine Blade. In 29th International Modal Analysis Conference. Jacksonville, FL.

Freebury, G. & Musial, W., 2000. Determining equivalent damage loading for full-scale wind turbine blade fatigue tests. In 19th ASME Wind Energy Symposium. Reno, NV.

Higdon, D., Gattiker, J., Williams, B., Rightley, M., 2008. Computer Model Calibration Using High-Dimensional Output. *Journal of the American Statistical Association*, 103(482), 570-583.

Jensen, F., Falzon, B.G., Ankersen, J., Stang, H., 2006. Structural testing and numerical simulation of a 34 m composite wind turbine blade. *Composite Structures*, 76(1-2), 52-61.

Kennedy, M. & O'Hagan, A., 2000. Predicting the output from a complex computer code when fast approximations are available. *Biometrika*, 87(1), 1 -13.

Larsen, F.M. & Sorensen, T., 2003. New lightning qualification test procedure for large wind turbine blades. In Proceedings of International Conference on Lightning and Static Electricity. Blackpool, UK.

Mandell, J.F., Samborsky, D.D., Wang, L., Wahl, N.K., 2003. New Fatigue Data for Wind Turbine Blade Materials. *Journal of Solar Energy Engineering*, 125(4), 506-514.

Marín, J.C., Barroso, A., Paris, F., Cañas, J., 2009. Study of fatigue damage in wind turbine blades. *Engineering Failure Analysis*, 16(2), 656-668.

Mollineaux, M., Van Buren, K. & Hemez, F., 2011. Simulating the Dynamics of Wind Turbine Blades: Part I, Model Development and Verification. In 13th AIAA Non-deterministic Approaches Conference. Denver, CO.

Noda, M. & Flay, R.G.J., 1999. A simulation model for wind turbine blade fatigue loads. *Journal of Wind Engineering and Industrial Aerodynamics*, 83(1-3), 527-540.

Paquette, J., van Dam, J. & Hughes, S., 2007. Structural Testing of 9 m Carbon Fiber Wind Turbine Research Blades. In 45th AIAA Aerospace Sciences Meeting and Exhibit. Reno, NV.

Paquette, J., Laird, D., Griffith, D.T., Rip, L., 2006. Modeling and Testing of 9m Research Blades. In 44th AIAA Aerospace Sciences Meeting and Exhibit. Reno, NV.

Paquette, J.A. & Veers, P.S., 2007. Increased strength in wind turbine blades through innovative structural design. In Proceedings, European Wind Energy Conference. Milan, Italy.

Resor, B., Paquette, J., Laird, D., Griffith, D.T., 2010. An Evaluation of Wind Turbine Blade Cross Section Analysis Techniques. In AIAA/ASME/ASCE/AHS/ASC Structures, Structural Dynamics, and Materials Conference. Orlando, FL.

Sørensen, B.F., Jørgensen, E., Debel, C.P., Jensen, F.M., Jensen, H.M., Jacobsen, T.K., Halling, K.M., 2004. Improved design of large wind turbine blade of fibre composites based on studies of scale effects., Risø National Laboratory.

Sutherland, H.J., Jones, P.L. & Neal, B., 2001. The Long-Term Inflow and Structural Test Program. In 2001 ASME Wind Energy Symposium. pp. 162–172.

Sutherland, H. & Kelley, N., 2003. Inflow and Fatigue Response of the Nwtc Advanced Research Turbine. In ASME Wind Energy Symposium. AIAA/ASME, pp. 500-510.

Van Buren, K., Mollineaux, M. & Hemez, F., 2011. Simulating the Dynamics of Wind Turbine Blades: Part II, Uncertainty Quantification and Model Validation. In 13th AIAA Non-deterministic Approaches Conference. Denver, CO.

Walford, C.A., 2006. Wind turbine reliability: Understanding and minimizing wind turbine operation and maintenance costs, Sandia National Laboratories.

White, J.R., Adams, D.E. & Rumsey, M.A., 2010. Modal Analysis of CX-100 Rotor Blade and Micon 65/13 Wind Turbine. In 28th International Modal Analysis Conference. Jacksonville, FL.

Wilson, G.E. & Boyack, B.E., 1998. The role of the PIRT process in experiments, code development and code applications associated with reactor safety analysis. *Nuclear Engineering and Design*, 186(1-2), 23-37.

# CHAPTER FOUR

# CONCLUSIONS

Presented in this thesis are the results from two studies that attempt to identify and quantify sources that degrade the predictive capabilities in finite element models of wind turbine blades. Understanding these sources in the FE model will allow for the development of reliable models in future studies of wind turbine blades.

First, the inherent incompleteness of numerical models is assessed through a study of *model form error*. Five FE models with varying levels of physics sophistication are developed in a comparative study. The *predictive maturity index (PMI)* is used as a metric to quantify the predictive capability of the alternative FE models. In practice, a wealth of experimental data is rarely available for calibration, therefore in this study only ten data points are used for the *synthetic experimental data*. Through PMI it is found that FE models with lower levels of physics sophistication have the ability to offer predictive capabilities that are comparable to those with higher levels of physics sophistication that are more computationally expensive. This study offers a proof of concept that can be used in future studies to quantitatively defend the level of physics sophistication that used in FE models of wind turbine blades.

Next, *model calibration* is performed through the use of **V**erification and **V**alidation exercises on the CX-100 wind turbine blade. In this study, first numerical uncertainty due to truncation errors is quantified. Next, sensitivity of the model parameters on model output is determined, and the imprecise parameters are calibrated using experimental evidence. Finally, the calibrated FE model is validated using a separate experimental dataset. With the validated FE model, damage scenarios at four locations around the blade are investigated: shear web

debonding at the top and bottom of the blade, leading edge erosion, and trailing edge delamination.